EPJ manuscript No.
(will be inserted by the editor)

Accumulation of particles in time-dependent thermocapillary flow in a liquid bridge. Modeling of experiments.

Melnikov Denis[1,a], Pushkin Dmitri[1], and Shevtsova Valentina[1]

Université Libre de Bruxelles, MRC, CP165/62, Av. F.D. Roosevelt, 50, B-1050, Bruxelles, Belgium

Abstract. The study addresses the phenomenon of accumulation of rigid tracer particles suspended in a time-dependent thermocapillary flow in a liquid bridge. We report the results of the three-dimensional numerical modeling of recent experiments [1,2] in a non-isothermal liquid column. Exact physical properties of both liquids and particles are used for the modeling. Two liquids are investigated: sodium nitrate ($NaNO_3$) and n–decane ($C_{10}H_{22}$). The particles are modeled as perfect spheres suspended in already well developed time-dependent thermocapillary flow. The particle dynamics is described by the Maxey-Riley equation. The results of our simulations are in excellent agreement with the experimental observations. For the first time we reproduced numerically formation of the particle accumulation structure (PAS) both under gravity and under weightlessness conditions. Our analysis confirms the experimental observations that the existence of PAS depends on the strength of the flow field, on the ratio between liquid and particle density, and on the particle size.

1 Introduction

A temperature gradient along the interface between two immiscible fluids causes variations of surface tension resulting in tangential stresses which can drive the bulk flow. This phenomenon is known as Marangoni convection. One of the simplest examples of a flow driven by the thermocapillarity is convection in plane non-isothermal layers or in liquid bridges. The liquid bridge is a liquid column with the cylindrical free surface suspended between two horizontal flat concentric disks. When a temperature difference ΔT is imposed at the bounding disks, both the surface tension gradient and buoyancy drive the convective motion.

The dynamics of the flow in a liquid bridge has been extensively studied. The steady flow at small temperature difference consists of a single toroidal vortex and the motion at the interface is directed downward from the hot upper disk to the cold lower one. Increase of ΔT above a certain critical value leads to an instability in the form of standing or azimuthally traveling hydrothermal wave. The value of the temperature difference, at which the onset of the instability occurs, is called the critical temperature difference ΔT_{cr}. Both the linear stability analysis and direct numerical simulations have shown dependence of ΔT_{cr} and of the supercritical flow regime upon the Prandtl number Pr (equal the ratio between the kinematic viscosity and the thermal diffusivity). The mechanism of the instability has been identified for each of them [3], [4]. The first instability for small Prandtl numbers is stationary. The branch for higher Prandtl numbers corresponds to an oscillatory instability. The bifurcation from a steady axisymmetric flow to a time-dependent one occurs via the Hopf bifurcation.

[a] e-mail: dmelniko@ulb.ac.be

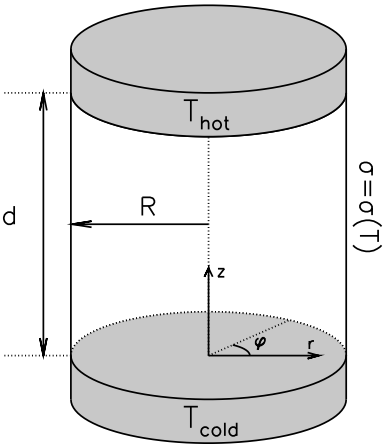

Fig. 1. Liquid bridge. Geometry of the problem.

When the Prandtl number is high, the hydrothermal waves are characterized by the azimuthal wave number m, which is integer ($m = 1, 2, 3, ...$) and strongly depends on the aspect ratio ($\Gamma = d/R$) of the column. For the temperature field, the azimuthal wave number m defines the number of the hot (cold) spots that are visible in the cross section and at the interface. In order to display these patterns we analyze the temperature perturbations. We obtain two-dimensional temperature fields by averaging the full field in the azimuthal direction [5] and subtract them from the full three-dimensional solution.

Particle tracing is among the most common approaches of visualizing the bulk liquid flow. A small amount of rigid tracers of relatively small size is mixed into the liquid, and their collective temporal and spatial behavior identifies the flow structure. A very interesting phenomenon was discovered by Schwabe and co-workers [6]: the rigid tracers did not follow the flow pattern but form stable spatial structures. This phenomenon was found in sodium nitrate and n–decane [1], [2] in liquid bridges of different aspect ratios.

The effect of accumulation of small rigid tracers in thermocapillary flow in liquid bridges (called particles accumulation structures, or PAS) occurs both under gravity and in weightlessness. Several research groups from Japan have experimentally studied this phenomenon in silicone oils of 2 cSt and 5 cSt, see [7], [8], [9]. Despite the extensive experimental studies a comprehensive theoretical explanation is stull lacking. This phenomenon occurs in far supercritical oscillatory flow regimes. Usually the imposed temperature difference ΔT should be high enough, about twice the critical value, in order to have a strong azimuthal flow. The flow must be laminar with a single (azimuthal) mode. Because at very high ΔT the flow undergoes transition to quasi-periodic and turbulent regimes and modes with several co-existing wave numbers m are observed [10], [11], appearance of a PAS is hardly, if at all, possible in such regimes.

Here we focus on reproducing numerically the experimentally observed periodical orbits (PAS) both under gravity and in weightlessness.

2 Mathematical model

The geometry of the problem is shown in Fig. 1. The liquid bridge consists of a fluid volume held between two differentially heated horizontal flat concentric disks of radius R, separated by a distance d. The temperatures T_{hot} and T_{cold} ($T_{hot} > T_{cold}$) are prescribed at the upper and lower solid-liquid interfaces respectively, yielding a temperature difference of $\Delta T = T_{hot} - T_{cold}$. The free surface is cylindrical and non-deformable.

The surface tension, liquid density and kinematic viscosity are taken as linear functions of temperature

$$\sigma(T) = \sigma(T_0) - \sigma_T(T - T_0),$$

$$\rho(T) = \rho(T_0)(1 - \beta_T(T - T_0)),$$
$$\nu(T) = \nu(T_0) + \nu_T(T - T_0),$$

where $\sigma_T = -\partial_T \sigma = const$, $\beta_T = -\frac{\partial_T \rho}{\rho(T_0)}$, $\nu_T = \partial_T \nu = const$, $\partial_T = \frac{\partial}{\partial T}$, T_0 is reference temperature. $T_0 = T_{cold}$ for the present study.

The governing Navier-Stokes, energy and continuity equations are written in non-dimensional primitive-variable formulation in cylindrical co-ordinate system.

$$\frac{\partial \mathbf{V}}{\partial t} + (\mathbf{V} \cdot \nabla)\mathbf{V} = -\nabla P + 2R_\nu \mathbf{S} \times \nabla(\Theta + z) + (1 + R_\nu(\Theta + z))\nabla^2 \mathbf{V} + Gr(\Theta + z)\frac{\mathbf{g}}{|\mathbf{g}|}, \quad (1)$$

$$\nabla \cdot \mathbf{V} = 0, \quad (2)$$

$$\frac{\partial \Theta}{\partial t} + (\mathbf{V} \cdot \nabla)\Theta + V_z = \frac{1}{Pr}\nabla^2 \Theta, \quad (3)$$

where velocity of the liquid is defined as $\mathbf{V} = V_r \mathbf{e_r} + V_\varphi \mathbf{e}_\varphi + V_z \mathbf{e_z}$. Radial, azimuthal and axial coordinates are denoted by r, φ and z respectively and $\mathbf{e_r}$, $\mathbf{e}_\varphi$, $\mathbf{e_z}$ are the basis vectors in the corresponding directions. The cylindrical co-ordinates (r, z) were scaled by the radius R and height d accordingly, and the velocity by $V_{ch} = \nu_0/d$, $\nu_0 = \nu(T_0)$. $\Theta_0 = (T - T_0)/\Delta T$ is the dimensionless temperature and Θ is the deviation from the linear temperature profile $\Theta = \Theta_0 - z$ (linear profile is subtracted). The scales for time and pressure are $t_{ch} = d^2/\nu_0$ and $P_{ch} = \rho_0 {V_{ch}}^2$, respectively ($\rho_0 = \rho(T_0)$). $\mathbf{S}$ is the strain rate tensor. $\mathbf{g}$ is the acceleration vector due to gravity. The following notations are used (F is a scalar field):

$$\text{Gradient} \qquad \nabla F = \Gamma \frac{\partial F}{\partial r}\mathbf{e_r} + \frac{\Gamma}{r}\frac{\partial F}{\partial \varphi}\mathbf{e}_\varphi + \frac{\partial F}{\partial z}\mathbf{e_z},$$

$$\text{Divergence} \qquad \nabla \cdot \mathbf{V} = \left(\frac{\Gamma}{r}\frac{\partial (rV_r)}{\partial r}, \frac{\Gamma}{r}\frac{\partial V_\varphi}{\partial \varphi}, \frac{\partial V_z}{\partial z}\right),$$

$$\text{Laplace operator} \qquad \nabla^2 F = \left(\frac{\Gamma^2}{r}\frac{\partial}{\partial r}\left(r\frac{\partial F}{\partial r}\right), \frac{\Gamma^2}{r^2}\frac{\partial^2 F}{\partial \varphi^2}, \frac{\partial^2 F}{\partial z^2}\right),$$

$$\text{Vector Laplacian} \qquad \nabla^2 \mathbf{V} = \left(\nabla^2 V_r - \Gamma^2 \frac{V_r}{r^2} - \frac{2}{r^2}\frac{\partial V_\varphi}{\partial \varphi}\right)\mathbf{e_r} + \left(\nabla^2 V_\varphi - \Gamma^2 \frac{V_\varphi}{r^2} + \frac{2}{r^2}\frac{\partial V_r}{\partial \varphi}\right)\mathbf{e}_\varphi + \nabla^2 V_z \mathbf{e_z},$$

where $\Gamma = d/R$ is the aspect ratio.

At the rigid walls non-slip conditions are used $\mathbf{V}(r, \varphi, z = 0, t) = \mathbf{V}(r, \varphi, z = 1, t) = 0$ and constant values of the temperature are imposed $\Theta(r, \varphi, z = 0, t) = \Theta(r, \varphi, z = 1, t) = 0$.

On the cylindrical free surface ($r = 1,\ 0 \le \varphi \le 2\pi,\ 0 \le z \le 1$), the free-slip conditions have the form:

$$V_r = 0 \ \text{ and } \quad 2(1 + R_\nu(\Theta + z))\, \mathbf{S} \cdot \mathbf{e_r} + Re\, (\mathbf{e_z}\partial_z + \mathbf{e}_\varphi \partial_\varphi)\, (\Theta + z) = 0.$$

The free surface is assumed thermally insulated

$$\partial_r \Theta(r = 1, \varphi, z, t) = 0.$$

The parameter R_ν describes the relative variation of viscosity, see [13]

$$R_\nu = \frac{\nu_T \Delta T}{\nu_0}, \ \ \nu = \nu_0(1 + R_\nu(\Theta + z))$$

The Prandtl, surface Reynolds and Grashof numbers are defined as:

$$Pr = \frac{\nu_0}{k}, \ \ Re = \frac{\sigma_T \Delta T d}{\rho_0 \nu_0^2}, \ \ Gr = \frac{g\beta_T d^3 \Delta T}{\nu_0^2}.$$

Table 1. Physical properties of $NaNO_3$ and of n-decane used for simulations.

	$NaNO_3$	$n-decane$
Density ρ_0, kg/m^3	1904	730
Kinematic viscosity ν_0, m^2/s	1.27×10^{-6}	1.17×10^{-6}
Thermal diffusivity k, m^2/s	1.58×10^{-7}	8.68×10^{-8}
Surface tension temperature coefficient σ_T, $N/(mK)$	7×10^{-5}	1.18×10^{-4}
Thermal expansion coefficient β_T, $1/K$	1.25×10^{-3}	1.06×10^{-3}

The surface Reynolds numbers is the analog of the Marangoni number $Ma = RePr$.

Two liquids were chosen for the study: sodium nitrate ($NaNO_3$) and n-decane ($C_{10}H_{22}$) with the Prandtl numbers equal accordingly to $Pr = 8$ and $Pr = 13.5$. Their properties could be found in [1] and [2]. Some properties are tabulated in Table 1. The aspect ratios were the same as in the experiments, i.e. $\Gamma = 0.68$ for $NaNO_3$ to obtain $m = 3$ and $\Gamma = 0.86$ for n-decane to have $m = 2$.

Considering viscosity as a linear function of temperature, R_ν is proportional to ΔT, i.e. ratio Re/R_ν is constant. The same is valid for the ratio Re/Gr.

The problem in the liquid bridge formed by $NaNO_3$ was considered under weightlessness. The viscosity was kept constant for this liquid, $\nu_T = 0$:

$$Re = 46.5\Delta T, R_\nu = 0, Gr = 0$$

The convection in the $C_{10}H_{22}$ liquid bridge was considered under Earth gravity. Viscosity in this case was temperature-dependent:

$$Re = 303.72\Delta T, Re/R_\nu = -2.6 \times 10^4, Re/Gr = -2.335$$

3 Solution method

The governing equations (1) - (3) were solved on a staggered non-uniform grid. For numerical simulations, the finite volume method in its cell-centers representation based on an explicit single time step marching method is applied. Central differences for spatial derivatives and forward differences for time derivatives are utilized for discretization of the partial differential equations. The finite volume method is chosen to fulfill the conservation laws within a truncation error of approximation of the governing equations. The computation of the velocity field at each time step is carried out with the projection method. A combination of fast Fourier transform in azimuthal direction and of an implicit ADI method at others is applied for calculating the Poisson equation for the pressure. More details on the used methods could be found in numerous books and articles, see for example [12].

Our in-house computational code has been developed about 10 years ago, and was successfully used for numerous studies of the thermocapillary flows in both small and large Pr liquids. The presented calculations were performed on two grids: on $[40 \times 32 \times 40]$ grid for sodium nitrate, and on $[40 \times 16 \times 40]$ for n-decane, where the numbers stay respectively for the amount of the grid cells in radial, azimuthal and axial directions. The grid is non uniform and refined in the near-boundary regions both in the radial and vertical directions, while it is uniform in the azimuthal one. The spatial resolution in the azimuthal direction is doubled in case of $NaNO_3$ because of the higher expected azimuthal wave number m. One can refer to e.g. [11], [13] for the code validation.

4 Particle tracing model

Particles with a finite size and mass have different dynamics from the surrounding fluid. Because of their inertia they do not evolve as point-like tracers. We employ the Maxey-Riley equation

[14] which was developed for the force balance of a dilute suspensions of rigid particles in a fluid. The force acting on a particle is a sum of the pressure-viscous force, the added mass force, the buoyancy force, the Stokes drag force, the Basset history force $\mathbf{F}_B$, external $\mathbf{F}_e$ and the Magnus $\mathbf{F}_m$ forces. We do not give them explicitly here.

$$\alpha\frac{d\mathbf{V}_p}{dt} = \frac{D\mathbf{V}}{Dt} - \frac{1}{2}\left[\frac{d\mathbf{V}_p}{dt} - \frac{D}{Dt}\left(\mathbf{V} - \frac{1}{10}\left(\frac{R_p}{d}\right)^2\nabla^2\mathbf{V}\right)\right] + (\alpha-1)\frac{Gr}{\beta_T\Delta T}\frac{\mathbf{g}}{|\mathbf{g}|}$$
$$-\frac{9}{2}\left(\frac{d}{R_p}\right)^2\left(\mathbf{V}_p - \mathbf{V} - \frac{1}{6}\left(\frac{R_p}{d}\right)^2\nabla^2\mathbf{V}\right) + \mathbf{F}_B + \mathbf{F}_e + \mathbf{F}_m, \quad (4)$$

here $\frac{D}{Dt} = \frac{\partial}{\partial t} + (\mathbf{V}\cdot\nabla)$ and $\frac{d}{dt} = \frac{\partial}{\partial t} + (\mathbf{V}_p\cdot\nabla)$, $\mathbf{V}_p$ and $\mathbf{V}$ are the velocity of a particle and of fluid respectively. $\alpha = \frac{\rho_p}{\rho_0}$ is particle to liquid density ratio, ρ_p is the density of the particle, R_p is its radius. μ and ν are the dynamic and the kinematic viscosity of the liquid.

In the absence of the external forces and assuming that the particles are not rotating, and that relative contributions of the added mass force (the second term in the right side of eq. (4)) and of the Stokes drag force are much larger than the Basset force F_B, one finally gets:

$$\alpha\frac{d\mathbf{V}_p}{dt} = \frac{D\mathbf{V}}{Dt} - \frac{1}{2}\left[\frac{d\mathbf{V}_p}{dt} - \frac{D\mathbf{V}}{Dt}\right] + (\alpha-1)\frac{Gr}{\beta_T\Delta T}\frac{\mathbf{g}}{|\mathbf{g}|} - \frac{9}{2}\left(\frac{d}{R_p}\right)^2[\mathbf{V}_p - \mathbf{V}]. \quad (5)$$

The right–hand side of simplified Eq. (5) describes the forces acting on a particle due to its interaction with the fluid (from left to right): the pressure–viscous force, the added mass force, the Stokes drag force, and the buoyancy force.

Two important points should be mentioned. First, is that the particles are non-intrusive, i.e. they do not change the liquid flow. Second, the particles are independent of each other and no interactions between them take place.

For the particle simulation, the flow field is required at an arbitrary point of the volume. To that end the velocity field was linearly interpolated on the computational grid, the details one may find in [15]. A special treatment is applied for particle behavior near the solid walls and the free surface. Non-elastic interaction of the particles with the rigid boundaries is assumed, i.e. a particle may approach to the wall on the distance of its radius. Then the particle is allowed to move along the wall or inside the liquid being consistent with the flow. The interaction with the free surface is also non-elastic. A particle can touch the interface from inside without crossing, i.e. the distance between the center of a particle and the interface cannot be smaller than the radius of the particle R_p.

The computer particle tracing was performed by introducing a few hundreds initially motionless rigid particles into the liquid volume. Like in the experiments diamond particles were used in case of $NaNO_3$. Their density is $3520kg/m^3$. However, small particles with density ratio $\alpha = 1.1$ were used in n-decane. We did not use heavy diamonds in this case for a reason explained below.

5 Results

5.1 Particles dynamics in sodium nitrate liquid bridge

Here we present numerical results for $NaNO_3$ melt with $Pr = 8$ as a test liquid under weightlessness. The liquid bridge radius is $R = 3\,mm$ and its length is $d = 2.04\,mm$, yielding the the aspect ratio of $\Gamma = 0.68$. The first target was to reproduce the traveling wave with azimuthal wave number $m = 3$, which was the experimental observation in [2]. Calculations give the value of the critical temperature difference of about $(18 \pm 0.1)K$. Direct numerical simulations of eqs. (1)-(3) were performed when the imposed temperature difference varied between $\Delta T_{cr} = 18K$ and $\Delta T = 60K$. Above the critical point the frequency of the hydrothermal wave is smoothly

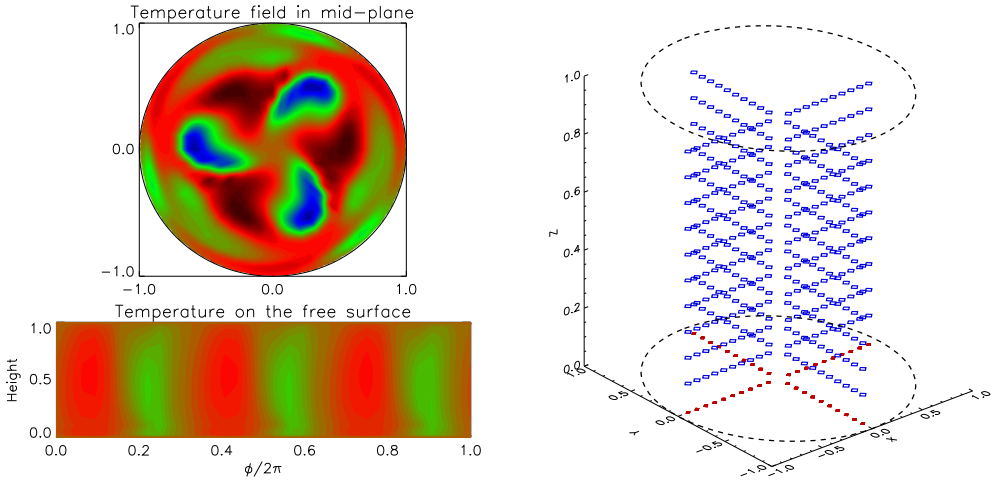

(a) **(b)**

Fig. 2. (a) Disturbances of temperature in mid-cross section and at unrolled interface at $\Delta T = 55K$. (b) Initial distribution of the particles being introduced to oscillatory flow shown by blue diamond symbols. Red diamonds are projections of the particles on the bottom.

growing from $f = 1.28\,Hz$ at $\Delta T = 20K$ to $f = 1.39\,Hz$ at $\Delta T = 60K$. The frequency was measured by recording the local fluctuations of the fluid temperature near the interface. Further increase of ΔT results in non-periodic regimes with more than one azimuthal wave number present in the spectrum, which is not acceptable for the formation of PAS. As in [2], the traveling wave with $m = 3$ was found and its thermal disturbance field is shown in Fig. 2(a). It consists of three cold and three hot spots rotating in counter clockwise direction.

Aiming at reproducing the particle accumulation structure, 400 diamond particles were introduced into the developed oscillatory flow in two perpendicular planes as shown in Fig. 2(b). Equation (5) was integrated about 20 viscous times τ_{vis} (one viscous time is equal to $d^2/\nu = 3.28\,s$), which corresponds to approximately one minute of experimental observation. The ratio of the density of the particles to that of $NaNO_3$ is rather large: $\alpha = 1.85$. A wide range of the particles size was numerically investigated. The radius of the particles was varied between $R_p = 5\mu m$ and $R_p = 70\mu m$. The PAS was found to exist in limited range of R_p at a given ΔT.

Figure 3 shows snapshots of the particles distribution in the bulk and their projections on the cold bottom at different ΔT for particle size $R_p = 20\mu m$. To imitate photo-like pictures of moving objects, the particles are shown in their movement by connecting two consecutive locations. Hence, the picture gives an idea about how fast and in which direction the particles are moving. Inside the oscillatory flow with $m = 3$ corresponding to $\Delta T = 35\,K$ the particles are distributed in the bulk and do not form the expected periodic orbit, see Fig. 3(a). Their projection on the bottom indicates that in the radial extension they are moving inside a ring near the interface and a small fraction is orbiting near the center. In the stronger flow, at $\Delta T = 55\,K$, the same particles form a closed thin loop, which looks like a bent wire, see Fig. 3(b).

The velocity near the free surface is higher than in the bulk. The particle orbit is steeper in the vicinity of the free surface and more horizontal elsewhere. Each particle is performing a combination of a rotation in $r - z$ plane and of a movement in the azimuthal direction. They are all moving independently, but at any instant they are located such that an illusion of a solid structure is created. The PAS is the same at any time instant, only rotating together with the hydrothermal wave. Comparing the results with the experimental observations, we may conclude that a very good agreement was achieved, see [1].

In the flow established at $\Delta T = 55K$, the PAS was observed for particles with radii up to $45\mu m$. We did not find PAS for larger particles.

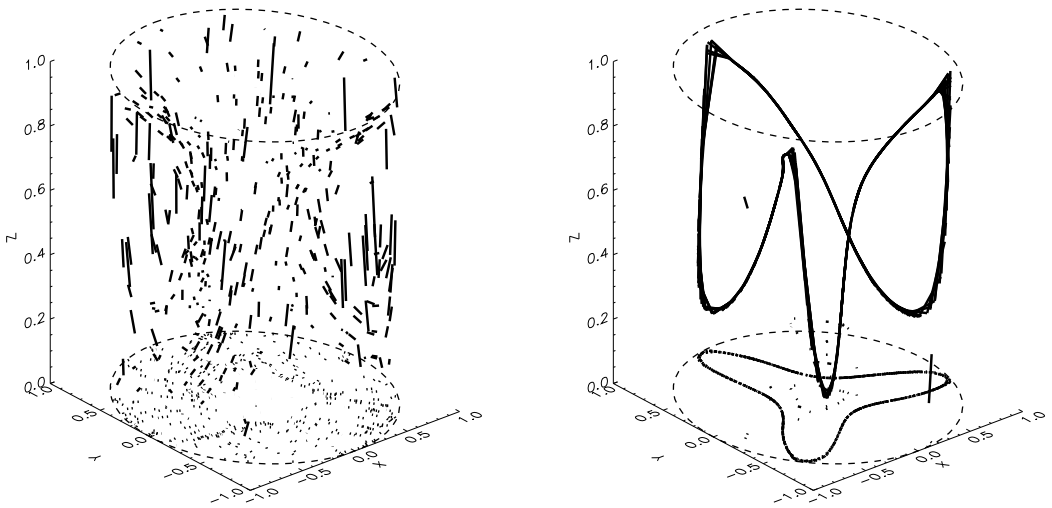

(a) **(b)**

Fig. 3. Snapshot of 400 particles of $R_p = 20\mu m$ size in radius in the oscillatory flow characterized by $m = 3$ at (a) $\Delta T = 35\,K$ when the particles do not accumulate in coherent structures; (b) $\Delta T = 55\,K$ when PAS is observed.

Table 2. Grid refinement study for the $NaNO_3$ liquid bridge at $\Delta T = 55\,K$.

Grid size	Grid spacing in radial and axial directions δr, (min, max)	δz, (min, max)	mode m	frequency $f(Hz)$	PAS for $20\mu m$ diamonds
$[40 \times 32 \times 40]$	(0.01, 0.04)	(0.02, 0.03)	3	1.34	Yes
$[60 \times 32 \times 80]$	(0.005, 0.03)	(0.005, 0.02)	3	1.33	Yes

To demonstrate the sufficiency of the resolution of the computational mesh, a grid refinement three-dimensional test was performed on another (finer) grid with $[60 \times 32 \times 80]$ cells. Numerical simulations of the supercritical flow at $\Delta T = 55\,K$ and the particle tracing for diamonds of the same size ($R_p = 20\mu m$) were repeated. The results are tabulated in Table 2.

A traveling hydrothermal wave with $m = 3$ was observed at $\Delta T = 55\,K$, with the frequency of $1.33\,Hz$ (Table 1). Figure 4 shows comparison of the particle distributions calculated on both grids. The comparison is made at 20 viscous times after beginning of the calculations with initial distribution of the particles shown in Fig. 2(b). On the $[60 \times 32 \times 80]$ grid with the better spatial resolution, the tracer particles also create a stable particle accumulation structure rotating azimuthally together with the traveling wave. The shapes of the PAS observed on the two grids are almost indistinguishable (compare the structures shown by red and blue symbols in Fig. 4), except that some particles got stuck at the hot corner when traced on the mesh with the better resolution, forming a sort of a discontinuous ring at the interface.

Through this grid refinement study, we have concluded that the grid density of the $[40 \times 32 \times 40]$ mesh is good enough for an accurate spatial resolution.

5.2 Particles dynamics in n-decane liquid bridge

The phenomenon of PAS was comprehensively studied in the oscillatory flow with $m = 3$, see e.g. [1], [7], [9], [16]. There were only a few experiments considering PAS in the flow with different azimuthal modes m. One of the goals of this section is to reproduce numerically the PAS in the flow with $m = 2$. For this purpose we closely follow the laboratory experiment by Schwabe et al. [1] in n-decane with $Pr = 13.5$ and $\Gamma = 0.86$ ($R = 3\,mm$ and $d = 2.58\,mm$). For

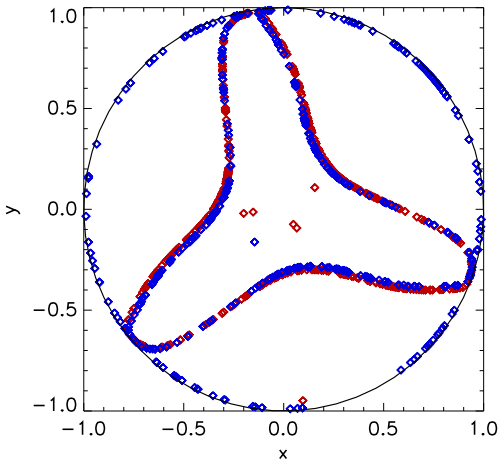

Fig. 4. Top view of distributions of 400 particles of $R_p = 20\mu m$ size in radius in the oscillatory flow at $\Delta T = 55\,K$. Red and blue symbols represent results obtained respectively on $[40 \times 32 \times 40]$ and $[60 \times 32 \times 80]$ grids.

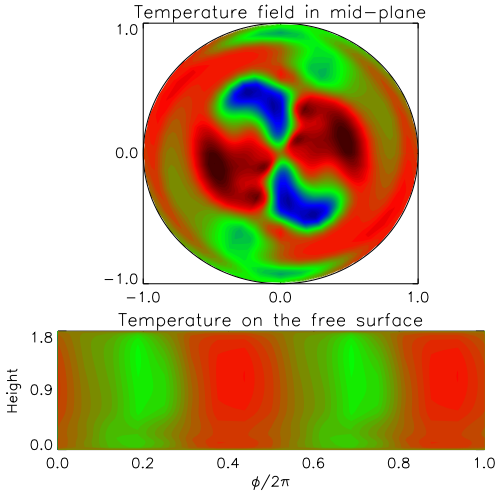

Fig. 5. Disturbances of temperature in mid-cross section and at unrolled interface at $\Delta T = 6K$.

these parameters we successfully reproduced the flow organization with azimuthal wave number $m = 2$. The disturbance flow is a $m = 2$ traveling wave, as shown in Fig. 5. Calculations give value of the critical temperature difference of about $(3.7 \pm 0.1)K$. Compared to Fig. 2 of Ref. [1], one may see that the calculated ΔT_{cr} is smaller than the reported experimental value (about $4.5K$ in the experiment). This discrepancy could be explained by the neglecting of several factors always present in the experiments and influencing the critical conditions, e.g. the interface deformation, non-zero heat exchange between the liquid and the surrounding gas, to mention a few.

It was very hard to obtain any particles accumulation structure in the n-decane liquid bridge. Different particles were tested, but only ones with the density 10 % larger than that of the liquid produced the PAS (Fig. 6). If the particles are too heavy, they either fall down to the bottom or get accumulated at the cold corner due to the presence of gravity. At the same time, the thermocapillary flow should be rather strong to keep heavy particles floating ($\Delta T = 6K$ only). The authors of the ground experiments also stated that sedimentation quickly settles all particles. They use an injection-retraction mechanism (syringe) to fill the liquid bridge and to mix the fluid from time to time (Prof. Schwabe, private communication).

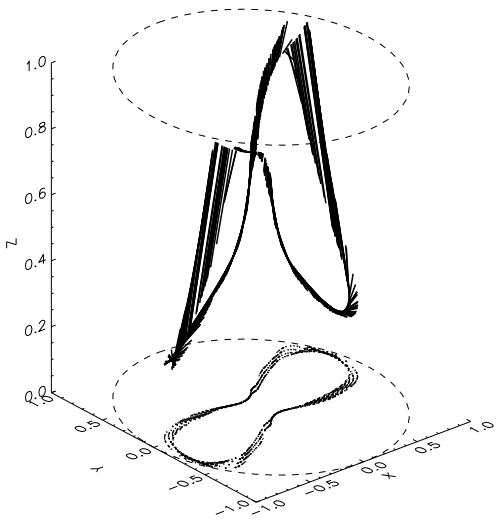

Fig. 6. Snapshot of 400 particles of $R_p = 30\mu m$ size in radius at $\Delta T = 6K$

Favorably, after integrating eq. (5) with $\alpha = 1.1$ during approximately 1 minute, the PAS was formed. The PAS was observed for the particles of radius of about $R_p = 20 - 30\mu m$. The PAS is shown in Fig. 6 and is characterized by $m_{PAS} = 2$. Figure 6 is produced in such a way that it imitates a photo of a moving object (similar to Fig. 3). The shape of PAS projection on the bottom is similar to those reported by Schwabe *et al.* (see Fig.5 in [1]).

At a slightly higher ΔT, i.e. at $7K$, the flow structure becomes more complex with more than one wave number m present in the spatial spectrum. As a result, the PAS has never been observed in the calculations for $\Delta T > 6\,K$.

6 Conclusions

We have successfully reproduced in computations the same flow organization as in the experiment, i.e. the azimuthally traveling wave with $m = 3$ for the case of sodium nitrate and $m = 2$ for n-decane. We favorably validated the numerical method carefully by analyzing the existence and the shape of particle accumulation structures on different spatial grids. A very good agreement, both qualitative and quantitative, with experimental observations has been achieved.

We have successfully modeled the particle accumulation structures, which were found in the experiments. Further work is planned aiming at analyzing the particles dynamics in order to determine the physical mechanism of PAS formation.

7 Acknowledgements

This work is supported by the PRODEX programme of the European Space Agency (ESA). The authors would like to thank Prof. D. Schwabe (University of Giessen, Germany) and Prof. J.C. Legros (ULB, Brussels) for valuable discussions.

References

1. Schwabe, D., Mizev, A., Tanaka, S., Kawamura, H., Microgravity Sci. and Technol. **18**, (2006) 117-127.
2. Schwabe, D., Mizev, A., Udhayasankar, M., Tanaka, S., Phys. of Fluids **19**, (2007) 072102.

3. Wanschura M., Shevtsova V.M., Kuhlmann H.C. and Rath, H.J., Phys. Fluids, **5**, (1995) 912-925.
4. Leypoldt, J., Kuhlmann H.C., and Rath, H.J., J. Fluid Mech., **414** (2000) 285-314.
5. Shevtsova V.M., Melnikov D.E. and Legros J.C., Phys. Review E., **68**, (2003) 066311.
6. Schwabe, D., Hintz, P. and Frank, S, Microgravity Sci. Technol., **9**, (1996), 163-168.
7. Nishimura, M., Ueno, I., Nishino, K., and Kawamura H., Exp. Fluids, **38** (2005) 285-290.
8. Tanaka, S., Kawamura, H., and Ueno, I., Phys. Fluids, **18**, (2006) 067103.
9. Abe, Y., Ueno I., and Kawamura H., Microgravity Sci. and Technol., **19**, (2007) 84-86.
10. Ueno, I., Tanaka S. and Kawamura, H., Phys. Fluids, **15**, (2003) 408-416.
11. Melnikov, D.E., Shevtsova, V.M., and Legros J.C., Phys. Fluids, **16**, (2004) 1746 - 1757.
12. Peyret, R. and Taylor, T. D., *Computational Methods for Fluid Flow*, Springer-Verlag, Berlin, (1990) 359 pp. Melnikov, D.E., Shevtsova, V.M., and Legros J.C., Phys. Fluids, **16**, (2004) 1746 - 1757.
13. Shevtsova V.M., Melnikov D.E. and Legros J.C., Phys. Fluids, **13**, (2001) 2851-2865.
14. Maxey, M. R. and Riley, J. J., Phys. Fluids, **26**, (1983), 883-889.
15. Melnikov, D.E., Shevtsova, V.M., FDMP(Fluid Dynamics and Material Processing), **1**, (2005) 189-199.
16. Ueno I., Abe, Y., Noguchi, K., and Kawamura H., Adv. Space Res., **41**, (2008) 2145-2149.